RSC Advances

ROYAL SOCIETY OF CHEMISTRY

www.rsc.org/advances

Photochemistry of methyl hypobromite (CH_3OBr): excited states and photoabsorption spectrum

Ljiljana Stojanović[b*], Gessenildo Pereira Rodrigues[b,c],

Saadullah G. Aziz[a], Rifaat H. Hilal[a,d*], and Mario Barbatti[b,e*]

[a] *Chemistry Department, Faculty of Science, King Abdulaziz University, Jeddah B.O. 208203, Saudi Arabia.*

[b] *Max-Planck-Institut für Kohlenforschung, Kaiser-Wilhelm-Platz 1, 45470 Mülheim an der Ruhr, Germany.*

[c] *Universidade Federal da Paraiba, 58059-900, João Pessoa-Paraíba, Brazil.*

[d] *Chemistry Department, Faculty of Science, Cairo University, Giza, Egypt.*

[e] *Aix Marseille Université, CNRS, ICR UMR7273, 13397 Marseille, France.*

[*]Corresponding authors; E-mails: stojanovic@kofo.mpg.de (LS), rhilal@kau.edu.sa (RH), mario.barbatti@univ-amu.fr (MB)

ABSTRACT

The singlet and triplet excited states of CH_3OBr with the excitation energies up to ~9.5 eV are studied using multi-reference configuration interaction with singles and doubles method (MRCI-SD) and several single-reference methods, including time-dependent density functional theory (TD-DFT), coupled-cluster (linear-response CC2 and equation-of-motion CCSD), and algebraic diagrammatic construction (ADC(2)). Among the single-reference methods, CCSD gives vertical excitation energies and oscillator strengths comparable to the MRCI-SD values for the majority of excited states. The absorption cross section in the gas phase in the region between 2 and 8.5 eV was simulated with CCSD using the nuclear ensemble approach. The computed spectrum predicts two intense absorption bands. The first band, peaked at ~7.0 eV, is induced by Rydberg excitation. The second band has a strong overlap between a broad σσ* transition and three Rydberg transitions, resulting in two peaks at 7.7 and 7.9 eV. The spectrum also features a low-intensity band peaked at ~4.5 eV due to nσ* excitation. The intensity of this band is influenced by spin-orbit coupling effects. We analyzed the dissociation pathways along O-Br and C-O coordinates by computing rigid potential energy curves of the ground and the lowest-lying singlet and triplet excited states, and discussed the possible dissociation products. Due to the specific electronic structure of the excited states, characterized by multireference, double excitations, and Rydberg states occurring in the low-energy region, their correct description along dissociation coordinates is feasible only with MRCI-SD.

Keywords: methyl hypobromite, excited states, photoabsorption spectrum.

INTRODUCTION

The discovery of the stratospheric ozone depletion in the late 1970s has brought a lot of attention to the photochemistry of chlorine and bromine organic compounds, as they have been noticed to play a significant role in stratospheric and tropospheric ozone depletion events. For instance, bromine compounds released from the Earth's surface reach the stratosphere, where they undergo photodissociation producing highly reactive species, such as atomic bromine (Br) or bromine monoxide (BrO). These reactive species interfere with natural ozone cycle, taking part as catalysts in the main chemical reactions in which ozone is depleted.[1-3] Even though bromine compounds are much less abundant than chlorine ones, it is estimated that they are more efficient in ozone destruction, causing significant fraction of the overall ozone loss.[4-6] In addition to its importance for ozone depletion processes, bromine radicals can also induce DNA damage.[7, 8] According to one of the proposed mechanisms, bromine radicals, which are usually formed in a tissue by reduction of bromate ions (BrO_3^-) by glutathione and Cystein (GSH/Cys), can induce one-electron oxidation of guanine. In this way cation radical of guanine are formed, and it is further subjected to a reaction with a water molecule and oxidation, yielding oxygenated derivatives of guanine.[7]

Methyl hypobromite (CH_3OBr), as a potential source of atomic bromine and bromine monoxide, is a molecule of interest for both ozone depletion and DNA damage. It is also the simplest prototype for organic hypobromites investigations. In spite of that, only a small number of theoretical and experimental studies have been devoted to elucidation of its electronic structure, absorption spectrum, and photochemical mechanisms.

In the first theoretical study on CH_3OBr, Guha and Francisco[9] investigated the geometry, vibrational spectrum, and energetics of CH_3OBr in the ground state using density functional theory (DFT), and computed vertical excitation energies to the six lowest-lying singlet excited states using

configuration interaction with singles (CIS). In their next computational study,[10] these authors reported vertical excitation energies to the five lowest-lying singlet and five lowest-lying triplet states computed with multi-reference configuration interaction with singles and doubles (MRCI-SD), as well as potential energy curves for these states along the O-Br coordinate computed with multi-configurational self-consistent field (MCSCF).

Later, Papayannis et al.[11] proposed six possible mechanisms for CH_3OBr decomposition. Based on unrestricted Møller-Plesset perturbation theory to the second order (UMP2), they optimized geometries and computed vibrational frequencies for reactants, transition structures, and products involved in the proposed decomposition channels. Finally, they also computed G2MP2 potential energy surfaces and used Rice-Ramsperger-Kassel-Marcus (RRKM) theory to estimate the microcanonical rate constants for each mechanism; concluding that the most important decomposition pathways are O-Br bond cleavage and 1,2-elimination pathway leading to HCHO and HBr.

To our knowledge, in the only existing UV-VIS spectroscopic study of CH_3OBr, Benter et al.[12] reported the gas-phase absorption spectrum restricted to the UVA region, between 230 and 400 nm, observing a week band with a peak at ~280 nm (~4.4 eV).

This series of physical-chemical studies have been of fundamental importance to our current understanding of the photochemistry of organic hypobromites. This investigation field, however, has been dormant for the last ten years and revisiting the photochemical properties of these compounds in terms of new methods and higher computational levels is especially timely.

Some of us have already taken the first steps in this direction. In a recent computational study, Aziz et al.[13] performed high-level coupled cluster (CCSD(T)), MP2, and DFT studies on the geometric features of tautomeric $CH_3OBr/CH_3BrO/BrCH_2OH$ and HCOBr(cis)/HCOBr(trans)/BrCHO systems. The latter tautomeric system is derived from the decomposition products of the former. Vibrational

frequencies were computed for all species and the topology of the electron density was analyzed using quantum theory of atoms in molecules (QTAIM).

In the present study, we turn to the excited-state properties, and investigate singlet and triplet excited states of CH_3OBr with the excitation energies up to ~9.5 eV, employing different correlated multi-reference and single-reference approaches. We compare the results obtained with single-reference methods and analyze their applicability for description of the excited states in the Franck-Condon region and along the O-Br dissociation coordinate. Since the CCSD describes correctly the vertical excitation energies of the molecule (except for few specific states, which will be discussed later), we employ this method together with the nuclear ensemble approach for the simulation of the UV photoabsorption cross section and action spectrum in the gas phase up to 8.5 eV. Furthermore, we study dissociation pathways of the molecule along O-Br and C-O bonds by computing the rigid potential energy curves of the ground and the low-lying excited states at MRCI-SD level.

This benchmark investigation not only provides significantly improved information about electronic structure and photochemistry of CH_3OBr, but it also reveals several challenges that further computational theoretical investigations must face for adequately describing the excited states of organic hypobromites. These challenges include low-energy double-excitations, bright valence states very sensitive to active spaces definition, innumerous very diffuse Rydberg states, and strong correlations out of the Franck-Condon region.

COMPUTATIONAL DETAILS

The ground state geometry of CH_3OBr molecule was optimized at the Møller-Plesset perturbation theory at the second order[14-17] (MP2) with aug-cc-pVTZ basis set[18, 19]. The C_s symmetry, theoretically confirmed in earlier studies[9, 11], was imposed in the geometry optimization and in all further

computations (except those for the absorption cross section). The optimized geometry of the molecule is given in the Supporting Information, Section S1. The molecule has trans (gauche) conformation. It is oriented such that Br, O, C, and one of the hydrogen atoms (H1) lie in the *xy*-plane, which coincides with the mirror plane, whereas the other two hydrogen atoms (H2 and H3) lie on the opposite sides of the *xy*-plane (Figure 1). The oxygen atom has a lone electron pair in a $2p_z$ orbital (out-of-plane), whereas two in-plane 2p orbitals take part in σ(O-Br) and σ(C-O) bonds. The bromine atom has two lone electron pairs, one in a $4p_z$ orbital (out-of-plane) and another one in an in-plane 4p orbital (a linear combination of $4p_x$ and $4p_y$ orbital). The other in-plane 4p orbital is involved in the σ(O-Br) bond.

We performed state-averaged multi-configurational self-consistent field (SA-MCSCF)[20, 21] computations of the ground and excited singlet and triplet electronic states. Separately one from another, fourteen singlet and fourteen triplet states (7A' and 7A") were computed at the SA-MCSCF level, averaging all states with equal weights. The diagonalization of the Hamiltonian was performed in the basis of configuration state functions (CSFs).

After a set of preliminary SA-MCSCF computations of potential energy curves of the ground and excited states along O-Br coordinate, we concluded that the CSFs formed by excitations of 12 active electrons within the active space composed of 11 orbitals [SA-MCSCF(12,11)] are necessary to describe the excited states of interest. The state-averaged molecular orbitals include seven valence and four Rydberg orbitals (within C_s group the occupied orbitals are 5a", 17a', 18a', 6a", and 19a', and the virtual orbitals are 20a", 21a", 8a", 22a', and 23a'). The σ(C-H) orbital, two linear combinations of σ(C-O) and σ(O-Br) orbitals, the symmetric and antisymmetric linear combination of $4p_z$ (Br) and $2p_z$ (O) orbitals (denoted further as n' and n"), the in-plane 4p orbital of Br (denoted as n_{Br}), and the σ*(O-Br) orbital comprise valence orbitals; and the Rydberg orbitals are mainly represented by 5s (Br), $5p_{xy}$ (Br), $5p'_{xy}$ (Br), $5p_z$ (Br) orbitals ($5p_{xy}$ and $5p'_{xy}$ are two linear combinations of bromine $5p_x$ and $5p_y$ orbitals).

A graphical representation of molecular orbitals in the active space and their compositions are given in the Supporting Information, Figure S1 and Table S1.

Analyzing the compositions of the electronic MCSCF wave functions, we have found that the CSFs obtained by double excitations to Rydberg orbitals do not contribute significantly to the composition of the excited states' wave functions for the studied O-Br stretching geometries. For this reason, we restricted the maximum number of excitations to these orbitals to one, reducing significantly computational time.

The state-averaged MCSCF wave functions were used as reference functions in the subsequent internally-contracted multi-reference configuration interaction with singles and doubles (MRCI-SD) computations[22-25]. Within MRCI-SD computations, the closed-shell orbitals were doubly occupied in all CSFs and they were not correlated through single and double excitations. The contribution of higher excitations corrections were taken into account by generalized Davidson's method (designated as MRCI-SD+Q). MCSCF and MRCI-SD computations were performed with MOLPRO 2012.1 code.[26]

We have computed spin-orbit matrix elements between fourteen singlet ((1-7)^{1}A′ and (1-7)^{1}A″) and fourteen triplet states ((1-7)^{3}A′ and (1-7)^{3}A″) employing state-interacting method implemented in MOLPRO code. The method implies the diagonalization of the sum of electronic and Breit-Pauli (BP) operator ($\hat{H}_{el} + \hat{H}_{BP}$) in the basis composed of MRCI-SD electronic wave functions. The transition dipole moments between the ground state and the obtained spin-orbit coupled excited states are computed.

Besides the multi-reference approach, we have tested the performance of single-reference methods, namely the full time-dependent density functional theory (TD-DFT) and Tamm–Dancoff approximation to the TD-DFT (TDA-DFT), three coupled cluster methods, and an algebraic diagrammatic construction method in the description of the excited states of CH_3OBr.

Linear-response (LR) TD-DFT and TDA-DFT computations were performed employing the long-range corrected density functionals CAM-B3LYP[27] and ωB97XD[28], which are proven[29, 30] to be more suitable for modeling electron excitations to delocalized orbitals, compared to hybrid functionals. These functionals are constructed to improve the long-distance behavior of the non-Coulombic part of the exchange functional. Moreover, the ωB97XD functional also includes dispersion correction, which may be important for description of the molecule in regions in which photodissociation occurs.

Among the coupled cluster methods, linear-response coupled cluster with approximated doubles and resolution-of-identity approximation (CC2)[31-33], equation-of-motion (EOM) coupled cluster singles and doubles (CCSD)[34-37], and completely renormalized equation of motion coupled cluster singles and doubles with noniterative triples correction (CR-EOM-CCSD(T))[38-40] computations were performed. Furthermore, computations were carried out with the linear-response algebraic diagrammatic construction method to approximated second order (ADC(2))[41, 42], using MP2 energies as the reference ground state. The CC2 and ADC(2) excited-state energies were computed with TURBOMOLE[43, 44]. TD-DFT, TDA-DFT, and CCSD computations as well as the geometry optimization at MP2 level were performed with Gaussian 09 software.[45] CCSD(T) computations were performed with GAMESS code.[46, 47]

Dunning's generally contracted aug-cc-pVTZ basis set was chosen for description of H, C, and O atoms, whereas in the case of bromine atom, the aug-cc-pVTZ basis set was augmented by a set of diffuse s, p, d, and f functions added in an even-tempered manner. The exponents for the additional diffuse functions are computed in the same way as in the case of Dunning's d-aug-cc-pVTZ set[48], which is developed for the elements of the first three rows of the periodic table. These exponents form a geometric progression with the exponents of the two most diffuse functions of the series, i.e. they are computed as $\alpha\beta$, where α is the exponent of the most diffuse function in the corresponding series of the aug-cc-pVTZ set and β is the ratio of the two most diffuse functions of the set.

The mentioned methods were used to compute the vertical excitation energies, oscillator strengths, and the O-Br potential energy curves of the ground and excited singlet and triplet states. C-O potential energy curves were also computed with MRCI-SD with the reference space discussed later. Besides that, the spatial extents (the expectation value of the operator $\langle r^2 \rangle$ in the electronic wave function ($\langle r^2 \rangle = \langle x^2 \rangle + \langle y^2 \rangle + \langle z^2 \rangle$)) of each of the studied electronic states were also computed using MCSCF and MRCI-SD wave functions at the ground state equilibrium geometry.

Finally, the UV photoabsorption cross section of the molecule was simulated using the nuclear ensemble approach[49] as implemented in the Newton-X code[50, 51]. 500 different nuclear geometries were sampled using a harmonic oscillator Wigner distribution (at 0 K) computed from harmonic normal modes in the ground state. Vertical excitation energies and oscillator strengths into eight excited singlet states were computed with EOM-CCSD method for each geometry in the ensemble. This information was used to compute the photoabsorption cross section, which was convoluted with normalized Lorentzian functions with a phenomenological width of 0.05 eV.

RESULTS AND DISCUSSION

In first three subsections, we present and discuss the vertical spectrum computed with different classes of methods. The focus of these sections is more technical, emphasizing the suitability of each method for dealing with this molecule. In the subsequent subsection, a more spectroscopic discussion is done. The last two sections deal with the photodissociation problem.

Vertical excitations with MCSCF and MRCI-SD

We present in Table 1 the results for the vertical excitation energies, oscillator strengths (for singlet states), main configuration weights, and $\langle r^2 \rangle$ values obtained at MCSCF and MRCI-SD levels, as well as vertical excitation energies obtained employing Davidson's correction for the singlet excited states of the CH_3OBr molecule. The results for the triplet states are presented in Table 2. Only the leading configurations with weights larger than 15% are shown and we simplify the states' assignment by not distinguishing between the different orbitals of the same type (for instance, both non-bonding n' and n'' orbitals are designated as n orbitals). A more detailed description of the excited states' wave functions in terms of configuration weights is given in the Supporting Information (Tables S2 and S3).

According to the MRCI-SD results, several intense electronic transitions are expected in the far-UV region, from 7 to 8 eV (Table 1). They correspond to the transitions to the ns Rydberg state ($3^1A''$), to the Rydberg states with mixed ns and np characters ($4^1A'$ and $5^1A'$), and to the σσ* state ($6^1A'$).

Most of the excited states are dominated by one configuration, for instance, the first several valence excited states (as $1^1A''$, $2^1A''$, $1^3A'$, $2^3A'$, and $1^3A''$) and the highest Rydberg states (as $7^1A'$, $6^1A''$, $7^3A'$, $7^3A''$). On the other hand, other states (for instance, $4^1A'$ and $5^1A'$) have multi-configurational character. The mixing of valence and Rydberg configurations occurs in the case of several excited states on MCSCF level, but the inclusion of additional correlation through MRCI-SD leads to a pure valence (for instance, $6^1A'$) or pure Rydberg character ($7^1A'$).

One of the most interesting features of the computed excited states is the occurrence of doubly-excited states even in a low-energy region, such as the $3^1A'$ and $5^1A''$ in the singlet manifold and the $5^3A'$, and $4^3A''$ in the triplet. These states are dominated by various valence $n^2\sigma^{*2}$ configurations, including all possible combinations of double excitations from n' and n'' orbitals to σ*(O-Br) orbital. Moreover, the wave functions of these states also include up to the 15% of mixed valence-Rydberg

doubly-excited configurations, $n^2\sigma^*p$ and $n^2\sigma^*s$ (see Table S2 and S3 in the Supporting Information). A large number of the remaining excited states also have up to 10% of double excitations. The existence of the excited states with significant contributions from double excitations in a low-energy region is not exclusive of this molecule and has also been predicted for other organic conjugated systems[52, 53].

On a more technical note, the effect of the dynamical correlation on the vertical excitation energies and wave functions of excited states can be elucidated comparing the results obtained with MCSCF and MRCI methods. The nature of the several excited singlet states changes upon inclusion of dynamical correlation at MRCI level. For instance, the $3^1A'$ state changes its character from np_z (within MCSCF) to the doubly-excited valence excited state ($n^2\sigma^{*2}$) (within MRCI), whereas the $5^1A'$ state, which is a doubly-excited valence state at MCSCF level, obtains a mixed ns-np_z Rydberg character at MRCI-SD level. The changes of the wave functions' compositions are accordingly reflected in the corresponding changes of $\langle r^2 \rangle$ values. Since Rydberg excited states generally have larger spatial diffuseness compared to valence states, their $\langle r^2 \rangle$ values are larger. Therefore, the change of the $3^1A'$ state's character from Rydberg to valence is accompanied by significant decreasing of the $\langle r^2 \rangle$ value.

The calculated MRCI-SD correlation energies, defined approximately by the differences between MRCI-SD and MCSCF energies ($E_{corr} = E(\text{MRCI-SD}) - E(\text{MCSCF})$), are given in Table S2 and Table S3 of the Supporting Information. The MRCI-SD correlation energies of the ground and valence excited states are larger than those of the states with mixed valence-Rydberg and Rydberg character. The valence excited states are more stabilized by additional dynamic correlation obtained within MRCI-SD than the Rydberg excited states, because in their case the larger number of electrons is correlated comparing to the Rydberg ones. The inclusion of additional electronic correlation through the MRCI-SD reduces the vertical excitation energies of valence excited states (for instance, $2^1A'$ and

1^1A"), and significant raises (from ~0.04 to ~0.88 eV) the vertical excitation energies of the excited states with Rydberg character, compared to the MCSCF results. Similarly, in the case of triplet states, additional correlation included by MRCI-SD mostly decreases the vertical excitation energies of the valence excited states and doubly-excited states, and increases the excitation energies of Rydberg states.

The extensivity correction included through the MRCI-SD+Q level does not significantly influence the excitation energies. The root-mean-square deviation (RMSD) between MRCI-SD+Q and MRCI-SD energies is 0.1 eV.

We show in the next sections that the MRCI-SD method predicts singlet and triplet σσ* energies that are 0.5 to 1.0 eV larger than those predicted by all other tested methods. It also predicts an oscillator strength for the singlet σσ* excitation that is about half of that given by the other methods. This deviation in the σσ* estimate can be noticed in the comparison between the MRCI-SD results and the single-reference methods in Figure 2-top. The good agreement between coupled-cluster, ADC, and TD-DFT methods for these quantities indicates that MRCI-SD may be providing inferior results for the σσ* state. Unfortunately, there are no available experimental results for comparison. Although we have not investigated this feature in detail, we have evidences (see next section) that the usage of a reduced active space, instead of the full valence space (which would be too computationally demanding), may be the reason underlying this problem.

Apart from the σσ* mismatch, the multireference character of the MRCI-SD, built upon active and reference spaces systematically deduced from a series of preliminary MCSCF computations, supports using the MRCI-SD results as the reference ones for the comparison with results of single-reference methods.

Spin-orbit coupling

As a relatively heavy atom, Br may induce spin-orbit coupling (SOC) effects in the electronic states. To assess them, we have computed the couplings between fourteen singlet ($(1\text{-}7)^1A'$, $(1\text{-}7)^1A''$) and fourteen triplet states ($(1\text{-}7)^3A'$, $(1\text{-}7)^3A''$) at MRCI-SD level. A summary of the spin-orbit effects on the singlet states after coupling to triplet states is provided in Table 3. Full information for all states is given in Table S4 of the Supporting Information.

The inclusion of spin-orbit coupling lifts the degeneracy of the triplet states; the initial fourteen triplet states result in 42 spin-orbit coupled states, where the energy separation between states arising from the same triplet state is $\sim 10^{-3} - 10^{-2}$ eV (Table S4). The spin-orbit interaction affects the vertical excitation energies of the majority of singlet states by less than 0.25 eV, except in the case of the highest states in the considered domain, whose energy shifts are very pronounced, up to 1.1 eV for the $6^1A'$ state and 1.6 eV for $7^1A'$ state. (The spin-orbit shifts of the triplet states follow similar trend.) These very large deviations for the high states, however, are most likely artifacts of the method and we will not draw any physical-chemical conclusion out of them.

Considering the values of oscillator strengths, the distribution of transition intensities among states is not changed significantly upon inclusion of spin-orbit effects. Transitions to the triplet state components have negligible oscillator strength values, except in the case of m = -1 component of $5^3A''$ state, for which the relatively large oscillator strength (f = 0.0110, Table S4) is induced by the singlet-triplet interaction with the close-lying $4^1A''$ state. The oscillator strengths for transitions to the singlet states are not significantly changed, except in the two anomalous cases of the $6^1A'$ and $7^1A'$ states. The effects of spin-orbit coupling on the photoabsorption spectrum of CH_3OBr will be further discussed in the "Photoabsorption spectrum simulation" Section.

Vertical excitations with TD-DFT

Since single-reference methods are widely used for describing excited states in general, we have tested their applicability for describing the excited states of CH_3OBr. We start by the popular LR TD-DFT, even though the occurrence of low-lying double excitations revealed by MRCI-SD preannounces the limitations of the method.

The results of the vertical excitation energies, oscillator strengths (for singlet states), and approximate configuration weights obtained with TD-DFT are shown for singlet excited states in Table 4 and for triplet excited states in Table 5. In the cases where it is not possible to quantify the contributions of individual configurations due to significant mixing of orbitals of different types (typically σ* and Rydberg s and p), only qualitative contributions are given. Moreover, we compare the vertical excitation energies and oscillator strengths for the transitions to excited states obtained by different methods in Figure 2 (top), and we show the correlation between the reference MRCI-SD vertical excitation energies of the singlet states and vertical excitation energies obtained using single-reference methods in Figure 2 (bottom).

As expected, the most striking discrepancy between TD-DFT and MRCI-SD results is the inability of TD-DFT method to reproduce doubly-excited states ($7^1A'$, $5^1A''$, $5^3A'$, and $6^3A''$ according to MRCI-SD results). Within the linear-response approximation, the susceptibility of a real interacting system is calculated from the susceptibility of its non-interacting Kohn-Sham counterpart and Hartree-exchange-correlation kernel[54]. The susceptibility of the Kohn-Sham system has poles only at single excitations, and in the adiabatic approximation (A) the Hartree-exchange-correlation kernel is frequency independent. Therefore, within LR ATD-DFT the susceptibility of the interacting system has poles only at single excitations and it is not able to reproduce the excited states with double excitation character[55].

In general, the vertical excitation energies and oscillator strengths of most of valence and low-lying Rydberg states obtained with TD-DFT are in a good agreement with MRCI-SD results. However, the vertical excitation energies of the highest Rydberg states (6^1A', 4^1A", 5^1A", and 6^1A") are significantly underestimated. Even though range separated functionals are constructed to give better description of delocalized states (as the Rydberg ones) by improving the asymptotic behavior of the exchange-correlation potential[56], they do not describe well these high-lying Rydberg states.

TD-DFT vertical excitation energies of σσ* states are significantly smaller than the corresponding MRCI-SD values (1.00 eV for ^{1}σσ* state and 1.09 eV for ^{3}σσ* state). TD-DFT also predicts significantly larger value of the oscillator strength for the transition to this state, compared to MRCI-SD value. As we already mentioned, in this case, we favor the TD-DFT results over those from MRCI-SD. Even though the σσ* character of this state is predicted by both TD-DFT and MRCI-SD, there is an important difference in compositions of the corresponding MRCI-SD and TD-DFT σ and σ* orbitals, which helps to understand the discrepancies in excitation energies and oscillator strengths. Within MRCI-SD, the σ orbitals are linear combinations of σ(O-Br) and σ(C-O) orbitals, whereas in the case of TD-DFT, the corresponding Kohn-Sham σ orbitals are more delocalized and have more complex compositions. This indicates that the active and reference spaces chosen for the MRCI-SD computations might not encompass all the orbitals relevant for description of σ orbitals, leading to the overestimation of the vertical excitation energies of σσ* states. Overall, ωB97XD performs slightly better than CAM-B3LYP. Excluding high Rydberg 5^1A" and 6^1A" states (according to TD-DFT assignation), the RMSD of the vertical excitation energies for the singlet states between TD-ωB97XD and MRCI-SD is 0.36 eV, whereas between TD-CAM-B3LYP and MRCI-SD it is 0.42 eV.

The vertical excitation energies of triplet states obtained with TD-DFT have significantly larger deviations from corresponding MRCI-SD results compared to the singlet states. The RMSD of the

vertical excitation energies for the triplet states obtained with ωB97XD functional and with MRCI-SD is 0.56 eV and the corresponding value for CAM-B3LYP functional is 0.61 eV.

The results of the TDA-DFT computations with CAM-B3LYP and ωB97XD are compared to the full TD-DFT results in Tables S5 and S6 in the Supporting Information. Even though it has been claimed that Tamm-Dancoff approximation to the full TD-DFT method could improve the description of triplet states,[57, 58] the obtained TDA-DFT vertical excitation energies of both singlet and triplet excited states are very close to their TD-DFT counterparts. For both functionals, the RMSD is only 0.05 eV for the singlet manifold and 0.12 eV for the triplet.

Vertical excitations with ADC(2), CC2, CCSD, CCSD(T)

The vertical excitation energies, oscillator strengths (for singlet states), and approximate configuration weights obtained with ADC(2), CC2, and CCSD are shown for singlet excited states in Table 6, and for triplet excited states in Table 7. Like for TD-DFT, wherever it is not possible to quantify the contributions of individual configurations due to the mixing of orbitals of different types, only the qualitative contributions are given.

ADC(2) and CC2 give very similar results for the vertical excitation energies and oscillator strengths of the studied excited states (the largest difference between corresponding vertical excitation energies obtained with ADC(2) and CC2 is ~0.04 eV). They describe well the several low-lying valence states with single excitation character (2^1A', 1^1A", and 2^1A"). Just like TD-DFT, they also predict vertical excitation energy for the $^1\sigma\sigma^*$ state smaller (by ~0.6 eV) than that given by MRCI-SD. The remaining states, which are mostly of Rydberg character and have partial doubly-excited character, are poorly described by both ADC(2) and CC2. Their vertical excitation energies and oscillator strengths remarkably deviate from the corresponding MRCI-SD values (see Figure 2). Furthermore, both ADC(2) and CC2 are not able to reproduce purely doubly-excited states.

One of the reasons for discrepancy between ADC(2)/CC2 and MRCI-SD vertical excitation energies for the states with partial doubly-excited character is that, within the ADC(2) and CC2, double excitations are treated approximately. In CC2, the doubles equations taken from CCSD are approximated by truncation to the first order of the fluctuation potential.[59] In the case of the ADC(2), it can be shown that its results are equivalent to those of the symmetrized Jacobian of the configuration interaction singles with iterative variant of the doubles correction (CIS(D_∞))[60]. Since CIS(D_∞) method is hierarchically lower than CC2, the approximations applied to the description of the double excitations within ADC(2) should be even stronger than in CC2.

Another pitfall that we have identified is that pure Rydberg $4^1A''$, $5^1A''$, and $6^1A''$ states are mainly described as mixed valence-Rydberg states with significant contribution of nσ* configurations (~20%) within ADC(2) and CC2, leading to a large deviation of their vertical excitation energies compared to the MRCI-SD values. As in the case of TD-DFT, the vertical excitation energies of triplet states have even larger deviations from their MRCI-SD counterparts.

CCSD brings significant improvement over ADC(2) and CC2 in the description of the excited states in the Franck-Condon region. The vertical excitation energies of the majority of the singlet states are in excellent agreement with MRCI-SD results. The mean deviation of the vertical excitation energies for the first nine CCSD singlet excited states from the corresponding MRCI-SD values is only 0.12 eV. The treatment of the states with partial doubly-excited character is improved compared to the CC2 method. However, as the other single-reference methods, CCSD is not able to predict the existence of pure doubly-excited states. This happens because while CCSD is correct to second order for single-electron excitations, it is correct only to the first order for double-electron excitations[59].

The vertical excitation energy of the σσ* state is also lower than the corresponding MRCI-SD value by ~0.5 eV. The computed CCSD oscillator strength value (0.1467) is much closer to the corresponding TD-DFT (0.1321) and CC2 (0.1360) values, than to the MRCI-SD value (0.0636).

The vertical excitation energies of the highest Rydberg $5^1A''$ and $6^1A''$ states (according to the CCSD assignment) are significantly underestimated compared to the MRCI-SD values.

A number of benchmark studies on organic molecules (for instance, on the set of organic chromophores[61], DNA nucleobases[62-64]) have shown that the EOM-CCSD(T) method gives correct descriptions of both localized and delocalized excited states. Comparing the vertical excitation energies of the singlet excited states obtained with CR-EOM-CCSD(T) and EOM-CCSD methods (Table 6), we conclude that triplet corrections do not affect significantly vertical excitation energies, except in the cases of the highest Rydberg $7^1A'$ and $7^1A''$ states, where it increases vertical excitation energies for 0.13 and 0.19 eV, respectively. The RMSD between CCSD and CCSD(T) energies is only 0.07 eV.

Photoabsorption spectrum simulation

Due to the high computational cost, which requires single point calculations of the vertical excitation energies and oscillator strengths for 500 molecular geometries distributed around the equilibrium geometry, we could not employ the MRCI-SD method in the photoabsorption cross section simulation. Instead, the simulation was done at CCSD level without including the spin-orbit coupling effects, which performs well near the Franck-Condon region. As already explained, the doubly-excited singlet $n^2\sigma^{*2}$ states (which correspond to the $3^1A'$ and $5^1A''$ states within C_s symmetry) could not be reproduced by this method. Because the oscillator strengths for excitations into these states are negligible, their absence among the CCSD excited states does not influence significantly the simulated spectrum.

The photoabsorption cross section of CH_3OBr simulated at CCSD level in the region from 2.5 to 8.5 eV is shown in Figure 3, including the contributions from the transitions to nine excited states ($(2\text{-}5)^1A'$ and $(1\text{-}4)^1A''$). We did not include the highest Rydberg states ($5^1A''$ and $6^1A''$), whose vertical excitation energies are underestimated, in the spectrum simulation.

The absorption spectrum has two high-intensity bands. The first intense band is peaked at ~7.0 eV and it is mostly induced by n-s (+n-p) excitation (transition to 3^1A" state according to CCSD results). The intense transition to the σσ* state gives a very broad contribution extending from 7 to 7.7 eV. The features at 7.35 and 7.5 are due to this transition, although they are most likely artifacts caused by statistical noise in the Monte-Carlo integration. The second intense band is mostly induced by an overlap of four transitions. The peak at 7.7 also has a large contribution from σσ*. The peak at ~7.9 eV is due three Rydberg states with mixed ns-np character (they are the 4^1A', 5^1A', and 5^1A" CCSD states within the C_s group).

Furthermore, in the low-energy region, the spectrum features a very low-intensity band with a peak at ~4.6 eV (it is shown in the inset of the Figure 3). Comparing the peak positions with the vertical excitation energies, one could conclude that the low-intensity band at ~4.6 eV is due to the nσ* excitation (transition to 2^1A' state).

We compared the obtained results in low-energy region with the experimental UV/VIS absorption spectrum[12] of CH_3OBr in the range from 400 to 230 nm (corresponding to ~3.1 to ~5.4 eV). They are shown together in the inset of the Figure 3. The experimental results reveal a very weak absorption band at 280 nm (4.43 eV) and 0.0016 $Å^2$.molecule^{-1} (52 M^{-1}.cm^{-1}). The position and width, and intensity of the low-intensity peak associated with nσ* transition obtained in the simulation agree very well with the experimental results, but the intensity of the simulated peak (0.0035 $Å^2$.molecule^{-1}) is overestimated by approximately a factor two compared to the experimental intensity. We will discuss the reason for this overestimation later in this section.

Under normal terrestrial irradiance, photoactivation of CH_3OBr should be restricted to the nσ* band at 4.6 eV. It is possible, however, that in extraterrestrial environments excitation of high-energy bands also contributes to the photoactivation. In fact, the action spectrum for extraterrestrial irradiance, computed as the product of the extraterrestrial solar irradiance[65] and the simulated absorption cross

section, shows that the ns+np band at 7 eV strongly contributes to the photoactivation too (Figure 3-bottom).

We analyze the effect of spin-orbit coupling on photoabsorption spectrum comparing the MRCI-SD vertical excitation energies and oscillator strengths of the eight excited states included in spectrum simulation in the cases with and without spin-orbit coupling (Table 3).

Mostly, the spin-orbit interaction induces the change of vertical excitation energies by less than ~0.2 eV. The spin-orbit interaction slightly increases the vertical excitation energy of $2^1A'$ state (~0.15 eV) and decreases its oscillator strength by approximately factor two. Thus, although the effect of the spin-orbit coupling on the position of the band at 4.6 eV (induced by the transition to $2^1A'$ state) is minor, it may substantially affect its intensity, reducing it by approximately factor two. Thus, the overestimation of the simulated intensity compared to the experimental intensity mentioned above can be attributed the lack of spin-orbit coupling effects in the CCSD photoabsorption spectrum simulations.

The first intense absorption band (peaked at ~7 eV) is not importantly affected by spin-orbit coupling, since the vertical excitation energy and oscillator strengths for the transition to $3^1A''$ state are not changed significantly upon inclusion of spin-orbit effects. Together with the reduction of the band intensity at 4.6 eV, we may expect a change of the relative importance of the two bands in the action spectrum shown in Figure 3-bottom, with lower intensity at 4.6 eV relative to the intensity at 7 eV.

Dissociation through O-Br and C-O cleavages

We investigated the mechanism of CH_3OBr decomposition that occurs through O-Br bond dissociation, by computing MRCI-SD stretching curves for the ground state and the thirteen lowest-lying singlet and triplet excited states ($(1\text{-}4)^1A'$, $(1\text{-}4)^3A'$, $(1\text{-}3)^1A''$, and $(1\text{-}3)^3A''$) of CH_3OBr.

As in the case of CH_3OCl (Ref.[66]), most of the computed excited states of CH_3OBr are strongly repulsive along the O-Br coordinate, indicating that O-Br bond cleavage is one of the favorable mechanisms, and agreeing with the conclusions of Papayannis et al.[11] based on chemical kinetics modeling.

The ground state and the first eleven excited states ($2^1A'$, $3^1A'$, $(1\text{-}3)^1A''$, $(1\text{-}3)^3A'$, $(1\text{-}3)^3A''$) converge to the same dissociation limit, yielding the CH_3O radical in the ground 1^2E state and Br atom in the ground ^2P state. The photodissociation in the higher $4^1A'$ and $4^3A'$ states yields CH_3O radical in the excited 1^2A_1 state and Br atom in the ground ^2P state (Figure 4). The computed excited states do not cross along the O-Br coordinate. Some of the pairs of singlet and triplet excited states (like $2^1A'$ and $2^3A''$, and $2^1A''$ and $2^3A'$) are quasi-degenerate along the O-Br coordinate.

Since among the suggested photodissociation mechanisms of CH_3OBr, the cleavage of the C-O bond has been also proposed[11], we also examined the behavior of the excited singlet and triplet states along C-O coordinate. The active space that has been chosen to describe the energies of excited states along the O-Br bond was not sufficient in the case of the C-O stretching. Therefore, we use somewhat larger active space composed of 13 active orbitals with 14 active electrons. Even at this level of theory, we could describe only the ground and the seven lowest-lying singlet and triplet states.

The rigid potential energy curves of five states ($1^1A'$, $2^1A'$, $1^1A''$, $1^3A'$, $1^3A''$), computed with MRCI-SD method, are shown in Figure 4. The ground and the first three excited states ($1^1A''$, $1^3A'$, $1^3A''$) exhibit the same dissociation limit producing CH_3 radical in the ground $1^2A''$ state and BrO radical in the ground $1^2\Pi$ state. In the dissociation limit, the higher $2^1A'$ state produces CH_3 radical in the ground $1^2A''$ and BrO radical in the $1^2\Sigma^-$ state.

Contrary to the potential energy curves along the O-Br coordinate, the lowest-lying excited states show minima along the C-O coordinate, indicating that in the case of photodissociation

mechanism that occurs through C-O bond cleavage, a potential energy barrier has to be overcome (the potential energy curves of CH_3OCl show similar behavior[66]). This fact implies that the C-O bond cleavage is a less probable mechanism compared to the O-Br cleavage.

Taking together these dissociation curves and the results for the absorption and action spectra, under terrestrial solar irradiation, where only the 4.6 eV band contributes to CH_3OBr photoactivation, we may expect CH_3O radicals to be formed exclusively in the 1^2E state. Above the ozone layer, however, under extraterrestrial irradiance, the action spectrum shows that the 7 eV band should also contribute to photoactivation. In this case, we may expect CH_3O radicals to be formed in both 1^2E and 1^2A_1 states. In any case, atomic Br should be released exclusively in the ^2P state.

Methods benchmark: O-Br cleavage

In the next subsections, we discuss the suitability of the applied single-reference methods for the description of excited states along O-Br stretching coordinate. MRCI-SD is taken as the reference method in all of the following comparative analysis. The potential energy curves of the first seven singlet and seven triplet excited states computed with MRCI-SD are shown in Figure 4. We restricted our computations to fourteen electronic states, because of root-flipping problems occurring in the SA-MCSCF computations of the potential energy curves, when higher electronic states intrude in state averaging.

O-Br dissociation with TD-DFT

The results for the potential energy curves computed with TD-ωB97XD method are shown in Figure 5 (the TD-CAM-B3LYP results are given in Figure S2 of the Supporting Information). Not surprisingly, TD-DFT does not describe correctly most of excited states in their dissociation limit (for example, $3^1A'$, $3^1A''$, $3^3A'$, and $3^3A''$), and the obtained potential energy curves exhibit incorrect topography. For

example, TD-DFT predicts an energy barrier for the dissociation in $4^1A'$ and $4^3A'$ states, states that are purely repulsive along O-Br coordinate according to MRCI-SD. TD-DFT also predicts the existence of several intersections in the singlet and triplet manifolds (for example, between $1^3A'$ and $1^3A''$ at 2.2 Å, Figure 5-bottom-left), which do not appear in MRCI-SD computations.

It is well-known[67, 68] that the description of excited states along dissociation coordinates poses a serious challenge to TD-DFT. These problems arise because the states gain more multi-reference character as the dissociation limit is approached and LR TD-DFT is not suited to deal with that. In fact, even the ground state along dissociation coordinate is already a challenge for DFT. The correlation effects in DFT are included through the *xc*-functional. In the cases of strong static correlations, such as the dissociation of bonds when near degeneracy effects arise, hybrid *xc*-functionals usually underestimate electronic correlation energy[69]. Since the description of the excited states within TD-DFT relies on description of the ground state, most of the excited states are not described correctly.

We analyzed the compositions of MRCI-SD electronic wave functions of the ground and excited singlet electronic states along the O-Br coordinate. An interesting feature is that the contribution of the doubly-excited CSFs to the ground state at the final point of the curve becomes significant (it reaches ~14%). Obviously, the electronic ground state becomes strongly correlated along O-Br coordinate, with doubly-excited configurations being of non-negligible importance, leading to the failure of the method.

These problems with strong correlation can be in principle alleviated by spin-unrestricted TD-DFT computations[70]. With this in mind, we computed the potential energy curves of the studied electronic states with TD-UDFT (ωB97XD) starting from broken-symmetry orbital guesses. As the potential energy curves for the singlet and triplet states show (Figure S3 of the Supporting Information), the additional electronic correlation recovered through spin-unrestricted approach does not significantly improve the description of the studied states.

O-Br dissociation with ADC(2), CC2, and CCSD

The corresponding potential energy curves computed with CC2 method are shown in Figure 5, whereas the results of ADC(2) and CCSD are shown in Figure S4 and Figure S5 of the Supporting Information. ADC(2), CC2, and CCSD, as single-reference methods, also experience problems with description of bond dissociations. Like TD-DFT, they all predict incorrect asymptotic behavior of several excited states and their potential energy curves exhibit incorrect topographies. This also includes the prediction of intersections along the stretching of the O-Br coordinate, which do not occur in the MRCI-SD results.

This behavior can also be explained by inability of these methods to describe correctly correlations appearing in the ground state along the dissociation curve. ADC(2) method is constructed upon MP perturbation theory, and thus it is expected that it can yield reasonable results only if the electronic ground state is described reasonably at the MP2 level, which excludes cases when ground state has pronounced multi-reference character. Likewise, the ability of CC2 and CCSD to describe the excited states relies on the performance of these methods for the description of the ground state.

The conclusions that ADC(2) and CC2 are not suitable for the computation of excited states along O-Br dissociation are supported by the D_1 diagnostic[71]. The D_1 values along the O-Br coordinate computed for MP2 and CC2 ground states are compared with their recommended limits in the Figure S6 in the Supporting Information. D_1 becomes very large along the O-Br coordinate (an order of magnitude larger than the recommended limit), which indicates that the ground state is not described well on MP2/CC2 levels.

CONCLUSIONS

In this study, the electronic structure of the CH_3OBr molecule is investigated by correlated single-reference and multi-reference methods. The excited singlet and triplet electronic states are computed at the equilibrium geometry of the ground state and along O-Br dissociation coordinate employing multi-reference configuration interaction with singles and doubles method, time-dependent density functional theory with range-separated functionals, algebraic-diagramatic-construction method, and coupled cluster methods. Spin-orbit coupled states are also computed at the multi-reference configuration level.

Most of the excited electronic states of CH_3OBr exhibit complex electronic structure, characterized by a mixing of several configurations. Moreover, doubly-excited configurations contribute significantly to the wave functions of several excited states even in a low-energy region. For these reasons, the correct description of the excited states in Franck-Condon region and beyond is a true challenge for the majority of the single-reference methods.

Among applied single-reference methods, CCSD describes the best most of the states dominated by single excitations in Franck-Condon region, with an exception of the highest Rydberg states lying above 8.5 eV ($5^1A''$ and $6^1A''$ according to the MRCI-SD assignation). ADC(2) and CC2 methods describe correctly the lowest-lying valence states, but underestimate the vertical excitation of the majority of the Rydberg states. TD-DFT, tested with two range-separated functionals, describes well most of the valence and the low-lying Rydberg excited states, but underestimates the excitation energies of the highest Rydberg states. All single-reference methods have failed to describe states with pure doubly-excited character. All these methods also provide very similar excitation energies and oscillator strengths for the bright $\sigma\sigma^*$, whose values are significantly different from those predicted by MRCI-SD. We believe that in this case MRCI-SD is providing the poorer results.

We simulated the UV photoabsorption cross section simulation with the nuclear ensemble approach, using vertical excitation energies and oscillator strengths into nine excited states computed with CCSD at the geometries sampled from a Wigner distribution. The inability of CCSD to reproduce the doubly-excited $3^1A'$ state does not significantly affect the simulated spectrum, since the predicted oscillator strength for the transition to this state is negligible. The computed photoabsorption cross section of the molecule is characterized by two intense bands in the region from 6.5-8.5 eV, and a low-intensity band with a peak at 4.6 eV. The position and width of peak at 4.6 eV is in excellent agreement with the available experimental spectral data, but its intensity is overestimated by a factor two, due to spin-orbit coupling effects. The simulated action spectrum for extraterrestrial solar irradiance indicates while near Earth surface photoactivation of CH_3OBr should be restricted to the 4.6 eV band, in the upper atmosphere the 7.0 eV bands should also significantly contribute to photoactivation.

Additionally, we investigated the dissociation pathways in the low-lying excited states along the O-Br and C-O bond cleavages using MRCI-SD method. The studied excited states are repulsive along the O-Br coordinate, implying that dissociation of O-Br bond occurs without energy barrier, and that decomposition after excitation should occur fast along this coordinate. On the other hand, most of the electronic states have minima along C-O coordinate, implying that this mechanism for dissociation is less probable compared to O-Br cleavage, because certain energy barrier to dissociation has to be surpassed to dissociate C-O bond. The analysis of dissociation curves together with the action spectrum indicates that while under terrestrial solar irradiation CH_3O radicals should be formed in a single state upon Br elimination, above the ozone layer this radical may be formed in two distinct electronic states.

Not surprisingly, the aforementioned pitfalls of single-reference methods to describe the vertical excitations become even more pronounced in the description of the potential energy curves of the excited states along the O-Br stretching coordinate. All methods provided very poor results compared to those at MRCI-SD. The reason for their inadequacy is the strong electronic correlations occurring in

the ground electronic state along the stretching. The inapplicability of single-reference methods in this case has been confirmed earlier for diverse other systems[72, 73]. For the correct description of the excited states in wide geometry range, a multi-reference method as the MRCI-SD seems to be mandatory.

ACKNOWLEGEMENTS

This Project was funded by the King Abdulaziz City for Science and Technology (KACST) under grant number 11-ENV 1995-03. The authors, therefore, acknowledge with thanks KACST for support for scientific research. Also, the authors appreciate the kind cooperation provided by the Deanship of Scientific Research (DSR), King Abdulaziz University. GPR acknowledges the Brazilian agencies CAPES and CNPq (Project 232180/2013-0), and the German agency DAAD for financial support. MB thanks the support of the A*MIDEX grant (n° ANR-11-IDEX-0001-02) funded by the French Government « Investissements d'Avenir » program.

REFERENCES

1. S. C. Wofsy, M. B. McElroy and Y. L. Yung, *Geophysical Research Letters*, 1975, **2**, 215-218.
2. F. S. Rowland, *Annual Review of Physical Chemistry*, 1991, **42**, 731-768.
3. M. J. Molina and F. S. Rowland, *Nature*, 1974, **249**, 810-812.
4. R. Hossaini, M. P. Chipperfield, S. A. Montzka, A. Rap, S. Dhomse and W. Feng, *Nature Geosci*, 2015, **8**, 186-190.
5. C. T. McElroy, C. A. McLinden and J. C. McConnell, *Nature*, 1999, **397**, 338-341.
6. T. G. Shepherd, D. A. Plummer, J. F. Scinocca, M. I. Hegglin, V. E. Fioletov, M. C. Reader, E. Remsberg, T. von Clarmann and H. J. Wang, *Nature Geosci*, 2014, **7**, 443-449.
7. M. Murata, Y. Bansho, S. Inoue, K. Ito, S. Ohnishi, K. Midorikawa and S. Kawanishi, *Chemical Research in Toxicology*, 2001, **14**, 678-685.
8. S. Ohnishi, M. Murata and S. Kawanishi, *Cancer Letters*, 2002, **178**, 37-42.
9. S. Guha and J. S. Francisco, *The Journal of Physical Chemistry A*, 1998, **102**, 9970-9974.
10. S. Guha, Y. Li and J. S. Francisco, *Chemical Physics Letters*, 2000, **330**, 195-198.
11. D. K. Papayannis, E. Drougas and A. M. Kosmas, *Chemical Physics*, 2002, **282**, 305-314.
12. T. Benter, C. R. Feldmann, U. Kirchner, M. Schmidt, S. Schmidt and R. N. Schindler, *Berichte der Bunsengesellschaft für physikalische Chemie*, 1995, **99**, 1144-1147.

13. S. Aziz, A. Alyoubi, S. Elroby, O. Osman and R. Hilal, *International Journal of Molecular Sciences*, 2015, **16**, 6783.
14. M. Head-Gordon, J. A. Pople and M. J. Frisch, *Chemical Physics Letters*, 1988, **153**, 503-506.
15. M. J. Frisch, M. Head-Gordon and J. A. Pople, *Chemical Physics Letters*, 1990, **166**, 275-280.
16. M. J. Frisch, M. Head-Gordon and J. A. Pople, *Chemical Physics Letters*, 1990, **166**, 281-289.
17. M. Head-Gordon and T. Head-Gordon, *Chemical Physics Letters*, 1994, **220**, 122-128.
18. T. H. Dunning, *The Journal of Chemical Physics*, 1989, **90**, 1007-1023.
19. A. K. Wilson, D. E. Woon, K. A. Peterson and T. H. Dunning, *The Journal of Chemical Physics*, 1999, **110**, 7667-7676.
20. P. J. Knowles and H.-J. Werner, *Chemical Physics Letters*, 1985, **115**, 259-267.
21. H. J. Werner and P. J. Knowles, *The Journal of Chemical Physics*, 1985, **82**, 5053-5063.
22. H. J. Werner and P. J. Knowles, *The Journal of Chemical Physics*, 1988, **89**, 5803-5814.
23. P. J. Knowles and H.-J. Werner, *Chemical Physics Letters*, 1988, **145**, 514-522.
24. P. Knowles and H.-J. Werner, *Theoret. Chim. Acta*, 1992, **84**, 95-103.
25. K. R. Shamasundar, G. Knizia and H.-J. Werner, *The Journal of Chemical Physics*, 2011, **135**, 054101.
26. H.-J. Werner, P. J. Knowles, G. Knizia, F. R. Manby, M. Schütz, P. Celani, T. Korona, R. Lindh, A. Mitrushenkov, G. Rauhut, K. R. Shamasundar, T. B. Adler, R. D. Amos, A. Bernhardsson, A. Berning, D. L. Cooper, M. J. O. Deegan, A. J. Dobbyn, F. Eckert, E. Goll, C. Hampel, A. Hesselmann, G. Hetzer, T. Hrenar, G. Jansen, C. Köppl, Y. Liu, A. W. Lloyd, R. A. Mata, A. J. May, S. J. McNicholas, W. Meyer, M. E. Mura, A. Nicklass, D. P. O'Neill, P. Palmieri, D. Peng, K. Pflüger, R. Pitzer, M. Reiher, T. Shiozaki, H. Stoll, A. J. Stone, R. Tarroni, T. Thorsteinsson, and M. Wang, *MOLPRO*, *version 2012.1*, *a package of ab initio programs*, see http://www.molpro.net.
27. T. Yanai, D. P. Tew and N. C. Handy, *Chemical Physics Letters*, 2004, **393**, 51-57.
28. J.-D. Chai and M. Head-Gordon, *Physical Chemistry Chemical Physics*, 2008, **10**, 6615-6620.
29. M. Isegawa, R. Peverati and D. G. Truhlar, *The Journal of Chemical Physics*, 2012, **137**, 244104.
30. A. D. Laurent and D. Jacquemin, *International Journal of Quantum Chemistry*, 2013, **113**, 2019-2039.
31. O. Christiansen, H. Koch and P. Jørgensen, *Chemical Physics Letters*, 1995, **243**, 409-418.
32. C. Hättig and A. Köhn, *The Journal of Chemical Physics*, 2002, **117**, 6939-6951.
33. C. Hättig and F. Weigend, *The Journal of Chemical Physics*, 2000, **113**, 5154-5161.
34. J. F. Stanton and R. J. Bartlett, *The Journal of Chemical Physics*, 1993, **98**, 7029-7039.
35. H. Koch and P. Jørgensen, *The Journal of Chemical Physics*, 1990, **93**, 3333-3344.
36. H. Koch, R. Kobayashi, A. Sanchez de Merás and P. Jørgensen, *The Journal of Chemical Physics*, 1994, **100**, 4393-4400.
37. M. Kállay and J. Gauss, *The Journal of Chemical Physics*, 2004, **121**, 9257-9269.
38. P. Piecuch, S. A. Kucharski, K. Kowalski and M. Musiał, *Computer Physics Communications*, 2002, **149**, 71-96.
39. K. Kowalski and P. Piecuch, *The Journal of Chemical Physics*, 2004, **120**, 1715-1738.
40. M. Włoch, J. R. Gour, K. Kowalski and P. Piecuch, *The Journal of Chemical Physics*, 2005, **122**, 214107.
41. A. B. Trofimov and J. Schirmer, *Journal of Physics B: Atomic, Molecular and Optical Physics*, 1995, **28**, 2299.
42. J. Schirmer, *Physical Review A*, 1982, **26**, 2395-2416.
43. R. Ahlrichs, M. Bär, M. Häser, H. Horn and C. Kölmel, *Chemical Physics Letters*, 1989, **162**, 165-169.

44. TURBOMOLE V6.6 2014, a development of University of Karlsruhe and Forschungszentrum Karlsruhe GmbH, 1989-2007, TURBOMOLE GmbH, since 2007; available from http://www.turbomole.com.
45. M. J. Frisch, G. W. Trucks, H. B. Schlegel, G. E. Scuseria, M. A. Robb, J. R. Cheeseman, G. Scalmani, V. Barone, B. Mennucci, G. A. Petersson, H. Nakatsuji, M. Caricato, X. Li, H. P. Hratchian, A. F. Izmaylov, J. Bloino, G. Zheng, J. L. Sonnenberg, M. Hada, M. Ehara, K. Toyota, R. Fukuda, J. Hasegawa, M. Ishida, T. Nakajima, Y. Honda, O. Kitao, H. Nakai, T. Vreven, J. A. Montgomery, Jr., J. E. Peralta, F. Ogliaro, M. Bearpark, J. J. Heyd, E. Brothers, K. N. Kudin, V. N. Staroverov, T. Keith, R. Kobayashi, J. Normand, K. Raghavachari, A. Rendell, J. C. Burant, S. S. Iyengar, J. Tomasi, M. Cossi, N. Rega, J. M. Millam, M. Klene, J. E. Knox, J. B. Cross, V. Bakken, C. Adamo, J. Jaramillo, R. Gomperts, R. E. Stratmann, O. Yazyev, A. J. Austin, R. Cammi, C. Pomelli, J. W. Ochterski, R. L. Martin, K. Morokuma, V. G. Zakrzewski, G. A. Voth, P. Salvador, J. J. Dannenberg, S. Dapprich, A. D. Daniels, O. Farkas, J. B. Foresman, J. V. Ortiz, J. Cioslowski, and D. J. Fox, *Gaussian 09*, *Revision D.01,*Gaussian, Inc., Wallingford CT, 2013.
46. M. W. Schmidt, K. K. Baldridge, J. A. Boatz, S. T. Elbert, M. S. Gordon, J. H. Jensen, S. Koseki, N. Matsunaga, K. A. Nguyen, S. Su, T. L. Windus, M. Dupuis and J. A. Montgomery, *Journal of Computational Chemistry*, 1993, **14**, 1347-1363.
47. M. S. Gordon and M. W. Schmidt, in *Theory and Applications of Computational Chemistry: the first forty years*, ed. C. E. Dykstra, G. Frenkling, K. S. Kim, G. E. Scuseria, Elsevier, Amsterdam, 2005, pp. 1167-1189.
48. D. E. Woon and T. H. Dunning, *The Journal of Chemical Physics*, 1994, **100**, 2975-2988.
49. R. Crespo-Otero and M. Barbatti, *Theor Chem Acc*, 2012, **131**, 1-14.
50. M. Barbatti, M. Ruckenbauer, F. Plasser, J. Pittner, G. Granucci, M. Persico and H. Lischka, *Wiley Interdisciplinary Reviews: Computational Molecular Science*, 2014, **4**, 26-33.
51. M. Barbatti, G. Granucci, M. Ruckenbauer, F. Plasser, R. Crespo-Otero, J. Pittner, M. Persico and H. Lischka, *NEWTON-X: a package for Newtonian dynamics close to the crossing seam, 2013*, Available via the Internet at www.newtonx.org.
52. J. H. Starcke, M. Wormit, J. Schirmer and A. Dreuw, *Chemical Physics*, 2006, **329**, 39-49.
53. R. J. Cave, F. Zhang, N. T. Maitra and K. Burke, *Chemical Physics Letters*, 2004, **389**, 39-42.
54. M. Petersilka, U. J. Gossmann and E. K. U. Gross, *Physical Review Letters*, 1996, **76**, 1212-1215.
55. N. T. Maitra, F. Zhang, R. J. Cave and K. Burke, *The Journal of Chemical Physics*, 2004, **120**, 5932-5937.
56. M. J. G. Peach, T. Helgaker, P. Salek, T. W. Keal, O. B. Lutnaes, D. J. Tozer and N. C. Handy, *Physical Chemistry Chemical Physics*, 2005, **8**, 558-562.
57. M. J. G. Peach, M. J. Williamson and D. J. Tozer, *Journal of Chemical Theory and Computation*, 2011, **7**, 3578-3585.
58. M. J. G. Peach and D. J. Tozer, *The Journal of Physical Chemistry A*, 2012, **116**, 9783-9789.
59. K. Sneskov and O. Christiansen, *Willey Interdisciplinary Reviews: Computational Molecular Sciences*, 2012, **2**, 566-584.
60. C. Hättig, in *Advances in Quantum Chemistry*, ed. H. J. Å. Jensen, Academic Press, 2005, vol. Volume 50, pp. 37-60.
61. B. Moore, H. Sun, N. Govind, K. Kowalski and J. Autschbach, *Journal of Chemical Theory and Computation*, 2015, **11**, 3305-3320.
62. P. G. Szalay, T. Watson, A. Perera, V. F. Lotrich and R. J. Bartlett, *The Journal of Physical Chemistry A*, 2012, **116**, 6702-6710.

63. P. G. Szalay, T. Watson, A. Perera, V. Lotrich, G. Fogarasi and R. J. Bartlett, *The Journal of Physical Chemistry A*, 2012, **116**, 8851-8860.
64. P. G. Szalay, T. Watson, A. Perera, V. Lotrich and R. J. Bartlett, *The Journal of Physical Chemistry A*, 2013, **117**, 3149-3157.
65. *ASTM E490-00a(2014), Standard Solar Constant and Zero Air Mass Solar Spectral Irradiance Tables*, ASTM International, West Conshohocken, PA, www.astm.org, 2014, (accessed September 2015).
66. Y. Li and J. S. Francisco, *The Journal of Chemical Physics*, 1999, **111**, 8384-8388.
67. O. V. Gritsenko, S. J. A. van Gisbergen, A. Görling and E. J. Baerends, *The Journal of Chemical Physics*, 2000, **113**, 8478-8489.
68. K. J. H. Giesbertz and E. J. Baerends, *Chemical Physics Letters*, 2008, **461**, 338-342.
69. O. V. Gritsenko, P. R. T. Schipper and E. J. Baerends, *The Journal of Chemical Physics*, 1997, **107**, 5007-5015.
70. D. Cremer, *Molecular Physics*, 2001, **99**, 1899-1940.
71. C. L. Janssen and I. M. B. Nielsen, *Chemical Physics Letters*, 1998, **290**, 423-430.
72. A. Dreuw and M. Head-Gordon, *Chemical Reviews*, 2005, **105**, 4009-4037.
73. A. Dreuw and M. Wormit, *Wiley Interdisciplinary Reviews: Computational Molecular Science*, 2015, **5**, 82-95.

TABLES

Table 1 SA-MCSCF, MRCI-SD, and MRCI-SD+Q results for vertical excitation energies (E_v in eV), spatial extent ($\langle r^2 \rangle$ in a_0^2), main configuration weights, and oscillator strengths (*f*) of the ground and excited singlet electronic states.

State	SA-MCSCF				MRCI-SD				MRCI-SD+Q
	E_v	weights	$\langle r^2 \rangle$	*f*	E_v	weights	$\langle r^2 \rangle$	*f*	E_v
$1^1A'$	0.00	0.95 gs	62.3	--	0.00	0.89 gs	64.1	--	0.00
$2^1A'$	4.91	0.76 nσ*	66.2	0.0055	4.77	0.74 nσ*	67.4	0.0012	4.70
$3^1A'$	7.10	0.78 np	131.6	0.0114	7.40	0.72 $n^2\sigma^{*2}$	68.3	0.0003	7.39
$4^1A'$	7.20	0.80 ns	112.4	0.0840	7.88	0.46 np + 0.27 ns	116.9	0.0301	8.01
$5^1A'$	7.31	0.71 $n^2\sigma^{*2}$	70.4	0.0000	7.95	0.52 ns + 0.35 np	118.6	0.0435	8.08
$6^1A'$	7.93	0.54 np + 0.26 σσ*	113.1	0.0566	8.14	0.57 σσ*	75.3	0.0636	8.12
$7^1A'$	8.05	0.34 np + 0.42 σσ*	93.2	0.0563	8.77	0.81 np	137.5	0.0007	8.92
$1^1A''$	3.69	0.80 nσ*	65. 6	0.0016	3.71	0.76 nσ*	66.3	0.0000	3.68
$2^1A''$	6.21	0.64 nσ*	70.5	0.0000	6.25	0.70 nσ*	66.4	0.0012	6.20
$3^1A''$	6.34	0.81 ns	105.5	0.0766	7.04	0.84 ns	107.2	0.0439	7.16
$4^1A''$	7.05	0.89 np	139.3	0.0000	7.81	0.72 np	126.5	0.0000	7.93
$5^1A''$	7.77	0.72 $n^2\sigma^{*2}$	67.5	0.0000	7.90	0.58 $n^2\sigma^{*2}$	77.9	0.0004	7.89
$6^1A''$	7.97	0.93 np	138.8	0.0066	8.82	0.88 np	137.2	0.0052	9.00
$7^1A''$	9.00	0.85 ns	110.4	0.0385	9.55	0.77 ns	107.2	0.0113	9.58

Table 2 SA-MCSCF, MRCI-SD, and MRCI-SD+Q results for vertical excitation energies (E_v in eV), spatial extent ($\langle r^2 \rangle$ in a_0^2), and main configuration weights of the excited triplet electronic states.

State	SA-MCSCF			MRCI-SD			MRCI-SD+Q
	E_v	weights	$\langle r^2 \rangle$	E_v	weights	$\langle r^2 \rangle$	E_v
$1^3A'$	4.46	0.85 nσ*	65.8	4.11	0.85 nσ*	66.2	3.97
$2^3A'$	6.13	0.89 σσ*	64.7	6.35	0.85 σσ*	64.8	6.37
$3^3A'$	7.15	0.93 np	113.6	7.85	0.86 np	104.2	7.98
$4^3A'$	7.17	0.90 np	124.7	7.91	0.84 np	130.3	8.05
$5^3A'$	7.94	0.93 np	133.1	8.69	0.79 $n^2\sigma^{*2}$	69.2	8.72
$6^3A'$	8.43	0.85 ns	125.8	8.70	0.87 np	130.5	8.81
$7^3A'$	8.57	0.83 $n^2\sigma^{*2}$	70.3	9.02	0.83 ns	131.2	9.09
$1^3A''$	3.30	0.88 nσ*	65.5	3.11	0.85 nσ*	65.5	3.02
$2^3A''$	6.10	0.78 nσ*	67.3	5.89	0.79 nσ*	66.0	5.76
$3^3A''$	6.37	0.99 np	104.8	6.99	0.82 np	103.0	7.11
$4^3A''$	7.19	0.90 np	132.7	7.75	0.68 $n^2\sigma^{*2}$	76.7	7.73
$5^3A''$	7.51	0.83 ns	125.6	7.88	0.74 np	124.0	7.94
$6^3A''$	7.88	0.76 $n^2\sigma^{*2}$	72.6	8.07	0.78 ns	129.7	8.11
$7^3A''$	8.07	0.93 np	132.4	8.85	0.88 np	132.0	9.01

Table 3 Vertical excitation energies (eV) and oscillator strengths for pure singlet states and for singlet states spin-orbit coupled to triplets. The same information for triplet states coupled to singlets is provided in the Supporting Information, Table S4.

	Without SOC		With SOC	
State	E_v	f	E_v^{SOC}	f
1A'	0.00	-	0.00	-
1A"	3.71	0.0000	3.73	0.0000
2A'	4.77	0.0012	4.93	0.0005
2A"	6.25	0.0012	6.23	0.0009
3A"	7.04	0.0439	7.05	0.0432
3A'	7.40	0.0003	7.45	0.0001
4A'	7.88	0.0301	7.94	0.0075
4A"	7.81	0.0000	8.01	0.0000
5A'	7.95	0.0435	8.11	0.0433
5A"	7.90	0.0004	8.13	0.0032
6A"	8.82	0.0052	9.00	0.0014
6A'	8.14	0.0636	9.25	0.0100
7A"	9.55	0.0113	9.60	0.0178
7A'	8.77	0.0007	10.35	0.1020

Table 4 TD-CAM-B3LYP and TD-ωB97XD results for vertical excitation energies (E_v in eV), configuration weights, and oscillator strengths (*f*) of the ground and excited singlet electronic states.

State	TD-CAM-B3LYP			TD-ωB97XD		
	E_v	weights	*f*	E_v	weights	*f*
$1^1A'$	0.00	gs	--	0.00	gs	--
$2^1A'$	4.37	0.98 nσ*	0.0010	4.43	0.98 nσ*	0.0009
$3^1A'$	7.14	0.92 σσ*	0.1297	7.19	0.92 σσ*	0.1321
$4^1A'$	7.524	ns + np	0.0550	7.60	ns + np	0.0486
$5^1A'$	7.64	ns + np	0.0111	7.62	ns + np	0.0195
$6^1A'$	8.30	ns + np	0.0040	8.37	ns + np	0.0211
$7^1A'$	8.34	ns + np	0.0380	8.38	ns + np	0.0190
$1^1A''$	3.45	0.98 nσ*	0.0000	3.49	0.98 nσ*	0.0000
$2^1A''$	6.01	0.96 nσ*	0.0003	6.03	0.95 nσ*	0.0003
$3^1A''$	6.74	ns + np	0.0563	6.83	ns + np	0.0591
$4^1A''$	7.40	ns + np	0.0005	7.51	ns + np	0.0000
$5^1A''$	7.58	ns + np	0.0093	7.59	ns + np	0.0065
$6^1A''$	8.17	ns + np	0.0000	8.20	ns + np	0.0007
$7^1A''$	8.30	ns + np	0.0091	8.32	ns + np	0.0091

Table 5 TD-CAM-B3LYP and TD-ωB97XD results for vertical excitation energies (E_v in eV) and configuration weights of excited triplet electronic states.

State	TD-CAM-B3LYP		TD-ωB97XD	
	E_v	weights	E_v	weights
$1^3A'$	3.38	0.96 nσ*	3.45	0.96 nσ*
$2^3A'$	5.26	0.96 σσ*	5.37	0.94 σσ*
$3^3A'$	7.40	ns + np	7.48	ns + np
$4^3A'$	7.57	ns + np	7.52	ns + np
$5^3A'$	8.21	ns + np	8.23	ns + np
$6^3A'$	8.28	ns + np	8.26	ns + np
$7^3A'$	8.29	ns + np	8.38	ns + np
$1^3A''$	2.54	0.97 nσ*	2.62	0.96 nσ*
$2^3A''$	5.18	0.92 nσ*	5.23	0.92 nσ*
$3^3A''$	6.64	ns + np	6.76	ns + np
$4^3A''$	7.33	ns + np	7.42	ns + np
$5^3A''$	7.55	ns + np	7.54	ns + np
$6^3A''$	8.08	ns + np	8.10	ns + np
$7^3A''$	8.26	ns + np	8.26	ns + np

Table 6 ADC(2), CC2, and CCSD results for vertical excitation energies (E_v in eV), configuration weights, and oscillator strengths (*f*) of the ground and excited singlet electronic states. The vertical excitation energies obtained with CCSD(T) are given as well.

State	ADC(2)			CC2			CCSD			CCSD(T)
	E_v	weights	*f*	E_v	weights	*f*	E_v	weights	*f*	E_v
1^1A'	0.00	gs	--	0.00	gs	--	0.00	gs	--	0.00
2^1A'	4.66	0.65 nσ*	0.0018	4.62	0.60 nσ*	0.0014	4.64	0.69 nσ*	0.0013	4.62
3^1A'	7.21	0.60 np	0.0204	7.21	0.60 np	0.0226	7.60	σσ* + ns	0.1467	7.60
4^1A'	7.52	0.56 σσ*	0.1387	7.53	0.56 σσ*	0.1360	7.90	ns + np	0.0354	7.91
5^1A'	7.74	0.43 nσ*+0.17 ns	0.0658	7.74	0.43 nσ*+0.17 ns	0.0674	7.92	ns + np	0.0430	7.91
6^1A'	7.99	0.72 np	0.0285	7.98	0.71 np	0.0347	8.68	ns + np	0.0439	8.66
7^1A'	8.52	0.46 np+0.08 ns	0.0018	8.51	0.45 np+0.07 ns	0.0027	8.76	ns + np	0.0007	8.89
1^1A"	3.63	0.57 nσ*	0.0000	3.61	0.57 nσ*	0.0001	3.68	0.65 nσ*	0.0000	3.68
2^1A"	6.29	0.35 nσ*+0.28 σσ*	0.0016	6.27	0.33 nσ*+0.29 σσ*	0.0008	6.29	nσ*+σσ*	0.0005	6.29
3^1A"	6.42	0.28 nσ*+0.13 ns	0.0380	6.41	0.29 nσ*+0.14 ns	0.0403	6.97	ns + np	0.0562	6.97
4^1A"	7.06	0.46 np+0.22 nσ*	0.0002	7.05	0.46 np+0.21 nσ*	0.0000	7.70	ns + np	0.0000	7.69
5^1A"	7.24	0.46 ns + 0.25 nσ*	0.0046	7.23	0.44 ns+0.24 nσ*	0.0061	7.87	ns + np	0.0103	7.86
6^1A"	7.87	0.28 nσ*+0.13 np	0.0002	7.86	0.28 nσ*+0.13 np	0.0001	8.49	ns + np	0.0000	8.47
7^1A"	7.96	0.41 nσ*	0.0067	7.95	0.41 nσ*	0.0075	8.63	ns + np	0.0103	8.82

Table 7 ADC(2), CC2, and CCSD results for vertical excitation energies (E_v in eV), configuration weights of the excited triplet electronic states.

State	ADC(2)		CC2		CCSD	
	E_v	weights	E_v	weights	E_v	weights
$1^3A'$	3.80	0.59 nσ*	3.77	0.59 nσ*	3.78	0.67 nσ*
$2^3A'$	5.95	0.57 σσ*	5.94	0.56 σσ*	5.82	0.59 nσ*
$3^3A'$	7.18	0.70 np	7.17	0.68 np	7.75	ns +np
$4^3A'$	7.61	0.44 nσ* + 0.16 ns	7.61	0.44 nσ* + 0.16 ns	7.80	ns +np
$5^3A'$	7.95	0.67 np	7.94	0.70 np	8.60	ns + np
$6^3A'$	8.44	0.44 np + 0.15 ns	8.43	0.44 np + 0.15 ns	8.64	ns +np
$7^3A'$	8.47	0.70 np	8.46	0.71 np	8.79	ns +np
$1^3A''$	2.87	0.56 nσ*	2.87	0.56 nσ*	2.90	0.64 nσ*
$2^3A''$	5.62	0.37 nσ* + 0.31 σσ*	5.61	0.37 nσ* + 0.31 σσ*	5.66	nσ* + σσ*
$3^3A''$	6.33	0.33 nσ* + 0.15 ns	6.32	0.33 nσ* + 0.15 ns	6.85	nσ* + ns + np
$4^3A''$	7.00	0.44 np	6.99	0.44 np	7.61	ns +np
$5^3A''$	7.23	0.43 ns	7.21	0.43 ns	7.84	ns +np
$6^3A''$	7.82	0.14 nσ* + 0.15 np	7.81	0.15 nσ* + 0.15 np	8.40	ns +np
$7^3A''$	7.93	0.42 nσ*	7.92	0.42 nσ*	8.58	ns +np

FIGURE CAPTIONS

Figure 1. Molecular structure of CH_3OBr alongside the atom labels.

Figure 2. Comparison of the vertical excitation energies and oscillator strengths of the excited singlet states obtained with different methods (top). Correlation between vertical excitation energies obtained with MRCI-SD (E_v^{MR}) and diverse single-reference methods (E_v^{SR}) (bottom). The results of an ideal SR method would lie on the diagonal.

Figure 3. Top: The simulated UV photoabsorption cross section of CH_3OBr. The first ionization potential (IP) computed with ωB97XD/aug-cc-pVTZ method is 10.06 eV. Inset: simulated cross section in low-energy region (black line) alongside the experimental result (red line). Bottom: Action spectrum for extraterrestrial solar irradiance.

Figure 4. The potential energy curves of the excited singlet and triplet states along O-Br (top) and C-O coordinate (bottom) computed with MRCI-SD. The initial geometry corresponds to the equilibrium geometry of the ground state.

Figure 5. The potential energy curves of the excited singlet (top) and triplet (bottom) states along O-Br coordinate computed with TD-ωB97XD method (left) and CC2 method (right). The initial geometry corresponds to the equilibrium geometry of the ground state.

FIGURES

Figure 1

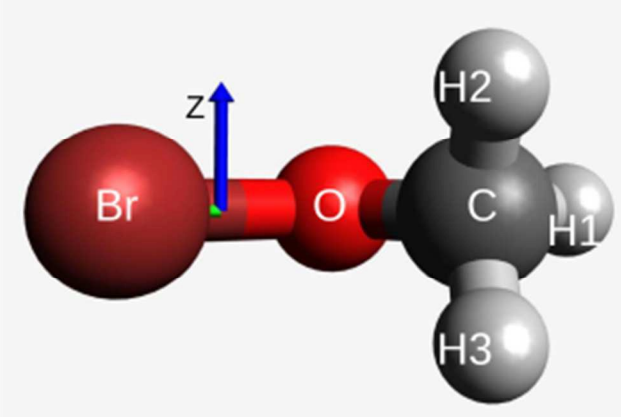

Figure 2

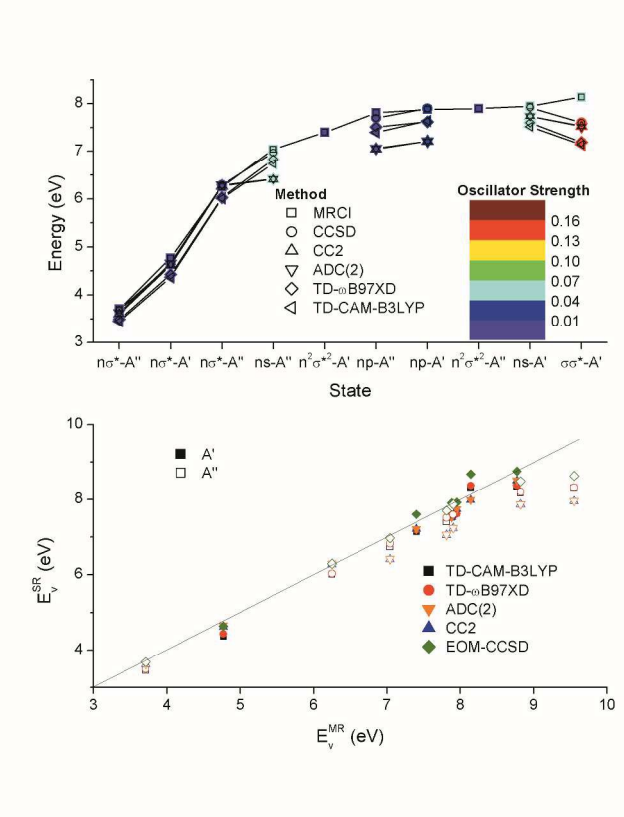

Figure 3

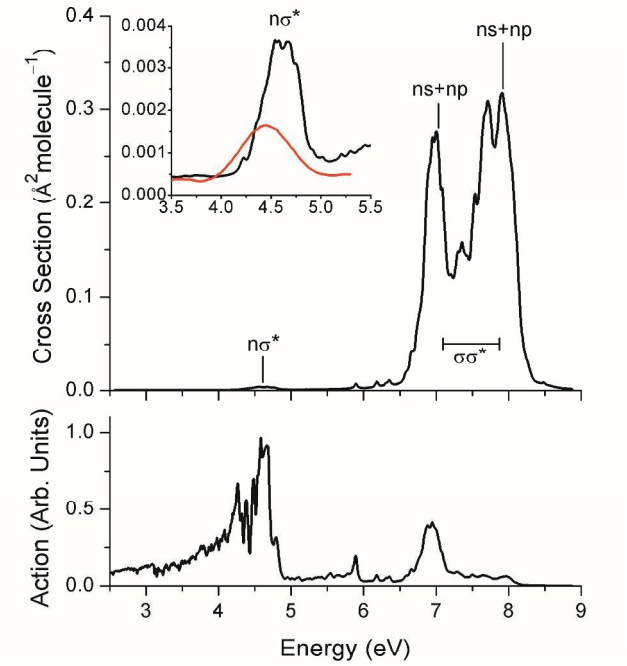

Figure 4

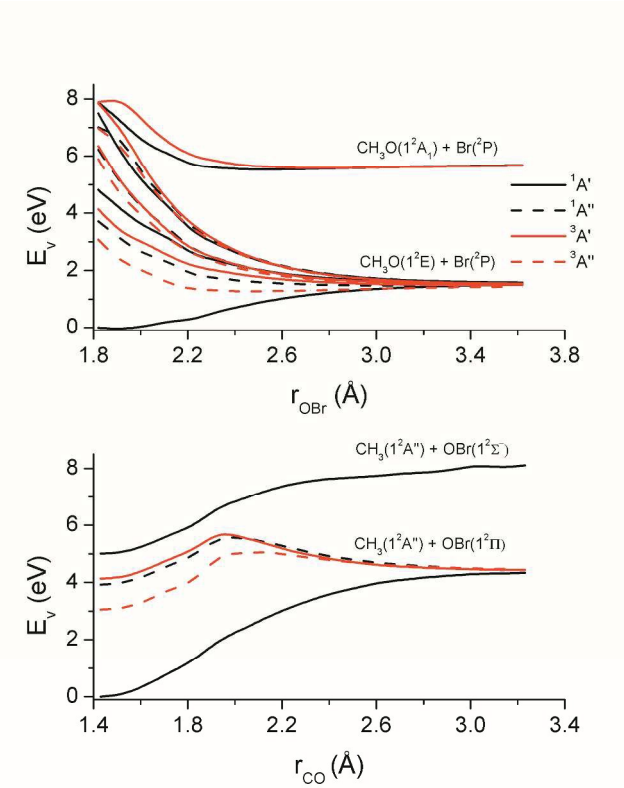

Figure 5

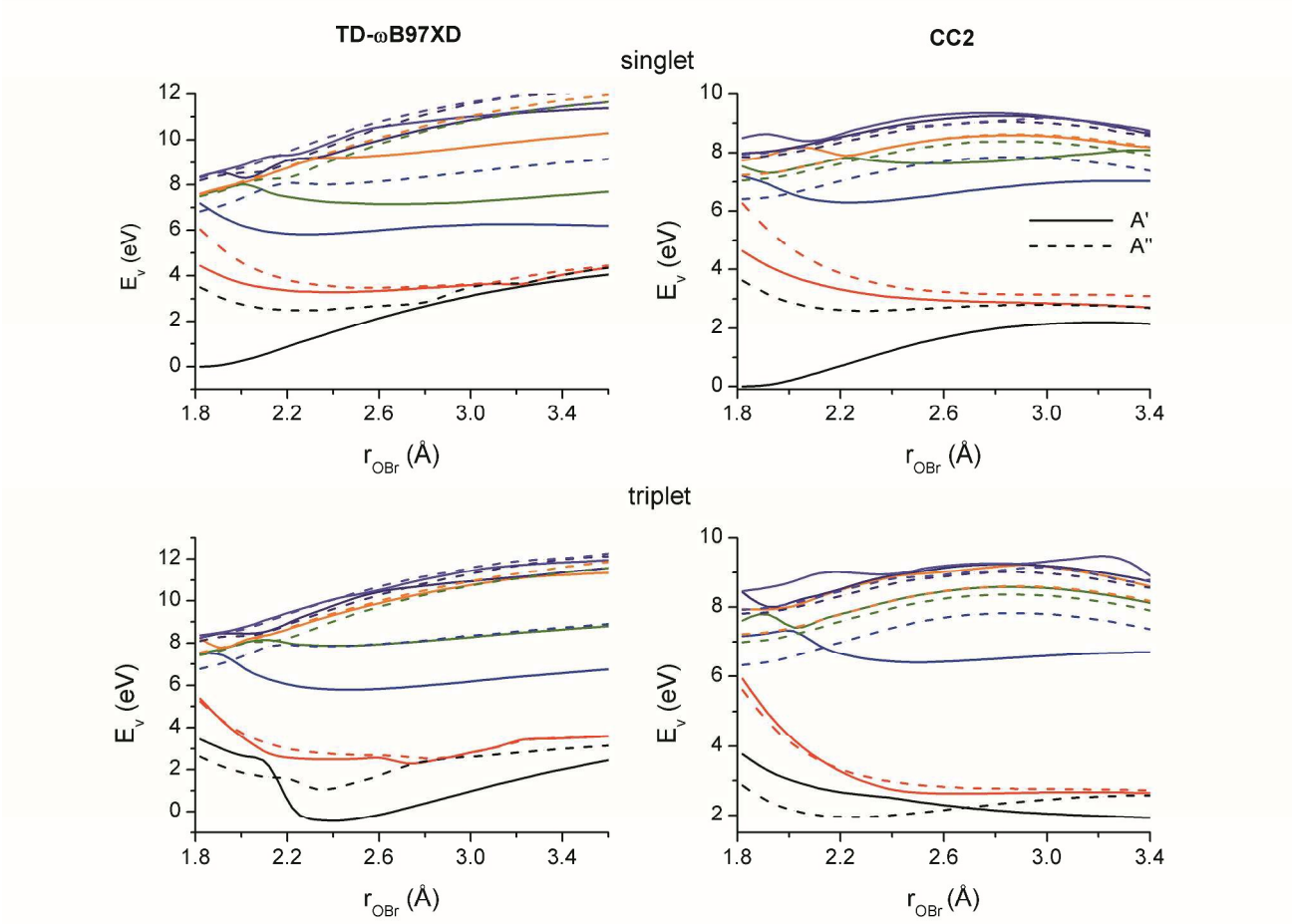

TABLE OF CONTENTS

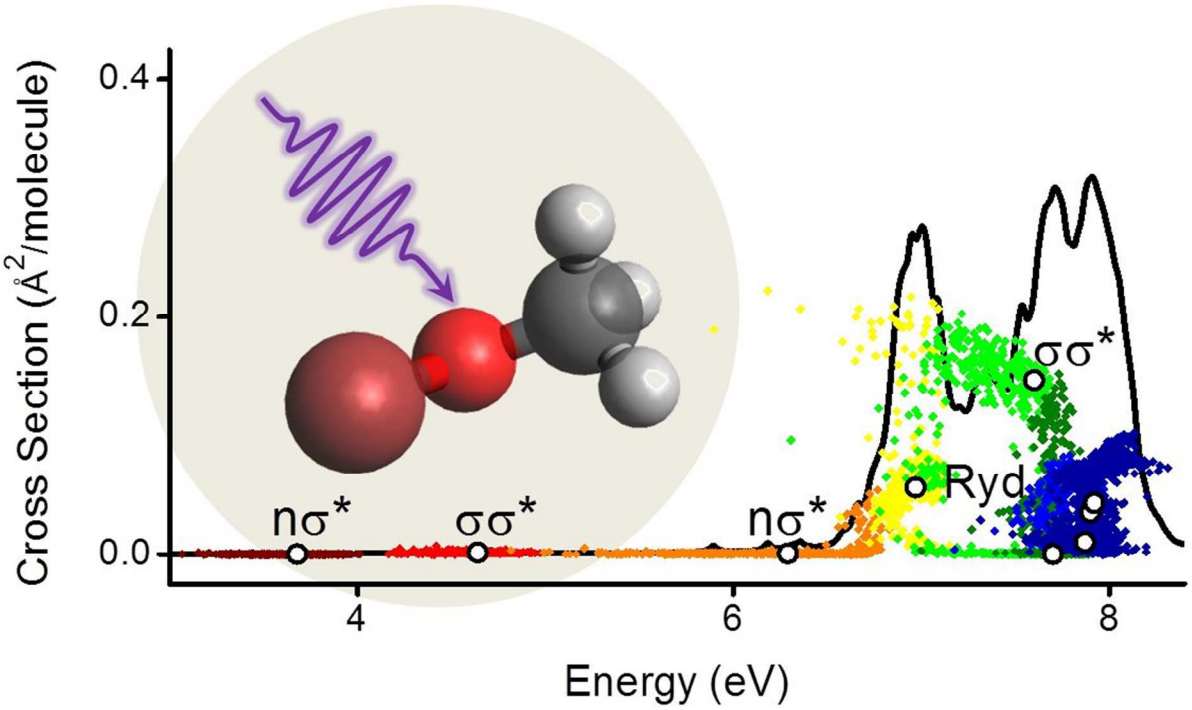

From photoabsorption to photodissociation, from MRCI to TDDFT; a comprehensive benchmark on the photochemistry of methyl hypobromite (CH3OBr) is provided.